

Cite this: DOI: 00.0000/xxxxxxxxxx

## Predicting stable lithium iron oxysulphides for battery cathodes

Bonan Zhu<sup>\*,a,b</sup> and David Scanlon,<sup>\*,a,b,c,d</sup>

Received Date

Accepted Date

DOI: 00.0000/xxxxxxxxxx

Cathode materials that have high specific energies and low manufacturing costs are vital for the scaling up of lithium-ion batteries (LIBs) as energy storage solutions. Fe-based intercalation cathodes are highly attractive because of the low-cost and the abundance of the raw materials. However, existing Fe-based materials, such as  $\text{LiFePO}_4$  suffer from low capacity due to the large size of the polyanions. Turning to mixed anion systems can be a promising strategy to achieve higher specific capacity. Recently, anti-perovskite structured oxysulphide  $\text{Li}_2\text{FeSO}$  has been synthesised and reported to be electrochemically active. In this work, we perform an extensive computational search for iron-based oxysulphides using *ab initio* random structure searching (AIRSS). By performing an unbiased sampling of the Li-Fe-S-O chemical space, several new oxysulphide phases have been discovered which are predicted to be less than 50 meV/atom from the convex hull and potentially accessible for synthesis. Among the predicted phases, two anti-Ruddlesden-Popper structured materials  $\text{Li}_2\text{Fe}_2\text{S}_2\text{O}$  and  $\text{Li}_4\text{Fe}_3\text{S}_3\text{O}_2$  have been found to be attractive as they have high theoretical capacities with calculated average voltages 2.9 V and 2.5 V respectively. With band gaps as low as about 2.0 eV, they are expected to exhibit good electronic conductivities. By performing nudged-elastic band calculations, we show that the Li-ion transport in these materials takes place by hopping between the nearest neighbouring sites with low activation barriers between 0.3 eV and 0.5 eV. The richness of new materials yet to be synthesised in the Li-Fe-S-O phase field illustrates the great opportunity in these mixed anion systems for energy storage applications and beyond.

### Introduction

The cathode is a critical component for lithium-ion batteries (LIBs) to achieve high energy density, safe operation, and economical viability. Despite many technological advances in LIBs, the cathode materials have barely evolved in the last 15 years. Those found in commercialised LIBs are still based on one of the three systems: layered  $\text{LiCoO}_2$ <sup>1</sup>, spinel  $\text{LiMn}_2\text{O}_4$ <sup>2</sup> and olivine  $\text{LiFePO}_4$ <sup>3</sup>, all of which were first proposed more than two decades ago. Iron-based cathode materials are very attractive as Fe is one of the most abundant transition metal in the upper crust with very low production costs. LIBs with olivine  $\text{LiFePO}_4$  cathodes

are nowadays used in applications including electric vehicles, but they suffer from relatively low specific energies<sup>4</sup>. Other iron based polyanion cathodes, such as  $\text{Li}_2\text{FeSiO}_4$ <sup>5,6</sup>,  $\text{LiFeSO}_4\text{F}$ <sup>7-9</sup> have also been proposed and shown to have comparable performance to  $\text{LiFePO}_4$ . The use of larger-sized polyanion groups, however, places an upper-limit on the energy density, which in turn offsets some of the benefits of the low cost. On the other hand, iron-oxide based cathodes suffer from the low voltage due to the  $\text{Fe}^{2+}/\text{Fe}^{3+}$  redox<sup>10</sup>, while attempts to utilize the  $\text{Fe}^{3+}/\text{Fe}^{4+}$  redox often leads to decomposition into other phases upon charging<sup>11-13</sup>.

Substituting one element with another has been a fruitful strategy for increasing the performance of cathode materials. Over the years, most of the research interests have been focusing on cationic substitution, and materials such as layered  $\text{LiNi}_x\text{Mn}_y\text{Co}_z\text{O}_2$ <sup>14</sup> have been reported to have improved reversible capacity over  $\text{LiCoO}_2$  - only half of the Li can be extracted in the latter. In the meantime, anionic substitution, or mixed anion materials have been largely unexplored until recently<sup>15</sup>. With different sizes, valence charge, electronegativity and polarizability of the anions, hetero-anionic materials are known to form layered structures due to preferential cation-anion bonding<sup>16,17</sup>.

<sup>a</sup> Department of Chemistry, University College London, 20 Gordon St, Bloomsbury, London WC1H 0AJ, United Kingdom. Email: bonan.zhu@ucl.ac.uk, d.scanlon@ucl.ac.uk.

<sup>b</sup> The Faraday Institution, Quad One, Becquerel Avenue, Harwell Campus, Didcot, OX11 0RA, United Kingdom.

<sup>c</sup> Thomas Young Centre, University College London, Gower Street, London WC1E 6BT, United Kingdom.

<sup>d</sup> Diamond Light Source Ltd., Diamond House, Harwell Science and Innovation Campus, Didcot, Oxfordshire OX11 0DE, UK

† Electronic Supplementary Information (ESI) available: additional phonon band structures, comparison of formation energy correction schemes and machine learned descriptor based finite-temperature stabilities. See DOI: 00.0000/00000000.

The incorporation of fluorine into oxide has been reported to improve the performance of disordered rock salt type cathodes<sup>18</sup>, as it offers another knob for tuning the valence of the transition metal cations, and being more electronegative than oxygen leads to higher voltages<sup>19,20</sup>. Anions that are less electronegative can be oxidised more easily than  $O^{2-}$ , which could favour anionic redox and leads to higher capacities<sup>21</sup>. For chalcogenide anions ( $S^{2-}$  and  $Se^{2-}$ ), the increased polarizability also give rise to better electronic conductivity than the oxide and polyanion based materials, which often poses limitations for fast and reversible Li cycling.

Recently, an anti-perovskite structured oxysulphide  $Li_2FeSO$  ( $Pm\bar{3}m$ ) was synthesised and found to have reasonably good electrochemical performance with a theoretical cationic redox capacity of 223 mAh/g, and a voltage of 2.5 V against graphite electrodes<sup>22,23</sup>. A subsequent computational study suggests that the anti-perovskite framework provides low lithium-diffusion barriers, and substituting Fe with other transition metal ions could lead to improved performance<sup>24</sup>. Replacing half of the Fe by Mn has been reported to improved the structural stability, although it leads to a decreased specific capacity<sup>25</sup>. Meanwhile, iron oxysulphide based cathodes have also been explored for applications in sodium-ion battery batteries<sup>26</sup>.

These findings beg the question: are there other oxysulphides waiting to be discovered? Computational materials discovery, and in particular, high-throughput screening studies, have previously been applied to many fields including battery cathodes<sup>27,28</sup>. Those studies, however, rely heavily on existing experimental data, as hypothetical materials are constructed from simple substitutions of the known materials<sup>17,29,30</sup>. For lithium iron oxysulphides, which remain largely unexplored so far, the available experimental data are scarce. The other way of discovering new materials is to directly search for low energy structures using first-principles calculations, with little or no experimental inputs<sup>31</sup>. Finding the lowest energy crystal structure is a challenging task, as it requires global optimisation over the high-dimensional configuration space. Many approaches have been developed to tackle the problem, including basin hopping<sup>32</sup>, minima hopping<sup>33</sup>, genetic algorithms<sup>34</sup> and particle-swarm optimisation<sup>35</sup>. In this work, we explore the lithium iron oxysulphide chemical space using *ab initio* random structure searching<sup>36,37</sup> (AIRSS), which is a simple, efficient and highly parallel method for searching for low energy structures. By sampling the Li-Fe-S-O space in an unbiased way, we have discovered many previously unknown phases that are both predicted to be relatively stable and have good electrochemical performances for cathode applications. Among those phases, two anti-Ruddlesden-Popper structured materials  $Li_2Fe_2S_2O$  and  $Li_4Fe_3S_3O_2$  are particularly attractive due to them being both nearly on the convex hull and have theoretical capacities exceeding that of the  $Li_2FeSO$ . Subsequent DFT calculations using the predicted crystal structures show that they have average voltages of 2.9 V and 2.5 V respectively, and band gaps about 2.0 eV. Using the climbing-image nudged elastic band method<sup>38,39</sup>, we show that both of them contains Li-diffusion networks with low transition state barriers similar to  $Li_2FeSO$ .

## Methods

Details about *ab initio* random structure searching (AIRSS) and its application to battery electrode materials can be found in the literature<sup>36,37,40,41</sup>. Briefly, this method searches for low energy structures by generating random but physically sensible initial structures followed by geometry optimisation using first-principles calculations. Unlike most other structure prediction methods, there is no iterative improvement process involved, hence the search can be parallelized and distributed over the computing resources easily. The plane wave density functional theory code CASTEP<sup>42</sup> is used for structure searching with a plane wave cut off energy of 340 eV and a k-point spacing of  $0.072\pi\text{\AA}^{-1}$  for sampling the reciprocal space. Core-corrected on-the-fly generated ultrasoft pseudopotentials from CASTEP's built-in QC5 library are used. Further DFT calculations are performed using the VASP<sup>43,44</sup> code with a plane wave cut off energy of 520 eV and a k-point spacing of  $0.042\pi\text{\AA}^{-1}$ . The PBE exchange-correlation functional<sup>45</sup> is used with the Hubbard correction applied for the *d* states of Fe. The *U* value for Fe is set to 4.0 eV based on the fitting of oxide formation energies<sup>46</sup>. A force-based convergence criteria of  $0.03\text{ eV \AA}^{-1}$  is used for all geometry optimisations, except when relaxing the input structure for phonon calculations where a tighter tolerance of  $0.0001\text{ eV \AA}^{-1}$  is applied. Ferromagnetic spin states have been assumed during the initial search to avoid complicating the energy landscapes. Enumerating spin arrangements for selected low energy phases shows that imposing anti-ferromagnetic orderings typically reduces the energy by 10 to 20 meV per atom, giving minor changes to the computed thermodynamic stabilities. Hence, the FM ordering is used in all further calculations for oxysulphides. Finite-displacement phonon calculations are performed using the Phonopy package<sup>47</sup> with an increased cut off energy of 650 eV. Climbing-image nudged elastic band<sup>38,39</sup> calculations are performed for determining the Li-diffusion barriers using the VTST code. The supercells are constructed such that periodic images of the Li-vacancy are more than  $10\text{ \AA}$  away in all directions. To avoid electron localisation upon creating a single Li vacancy, which would otherwise complicate the potential energy surface and the minimum energy pathway, a single electron is removed from the supercell with a neutralising background added. This resembles the case where the polaron formed is far away from the Li-vacancy. The AiiDA framework is used to automate the DFT calculations and preserve their provenance<sup>48,49</sup>.

## Results and Discussion

### New phases in the Li-Fe-O-S space

The full Li-Fe-O-S chemical space can be represented as a tetrahedron with vertices being the elemental species, as shown in Fig. 1. In oxysulphides, both oxygen and sulphur typically have the  $-2$  oxidation states. For metal cations, Li is expected to be in the  $+1$  state and we limit Fe to be in the  $+2$  and  $+3$  states. To maintain charge neutrality, the sum of the oxidation states for a given composition should be zero. This means that the compositions to be searched are located on two cross-sectional planes of the full Li-Fe-S-O tetrahedron: one for those with Fe in  $+3$  and the

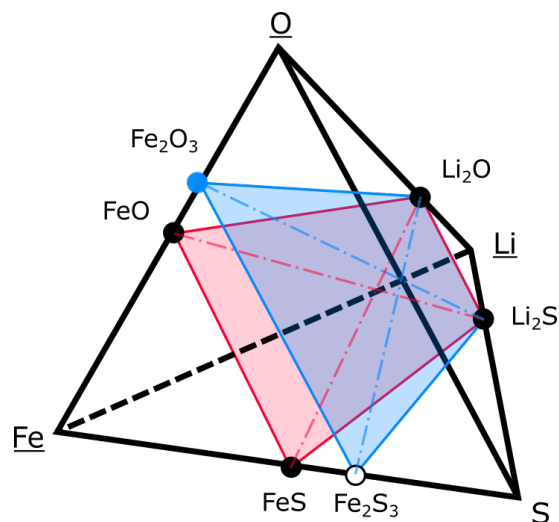


**Fig. 1** A tetrahedron representing the Li-Fe-S-O chemical space. charge-neutral compositions with formal valences (Fe: +2/+3, Li: +1, S: -2, O: -2) for oxysulphides are located on the two planes with Fe in +3 (red) and +2 (blue) states.

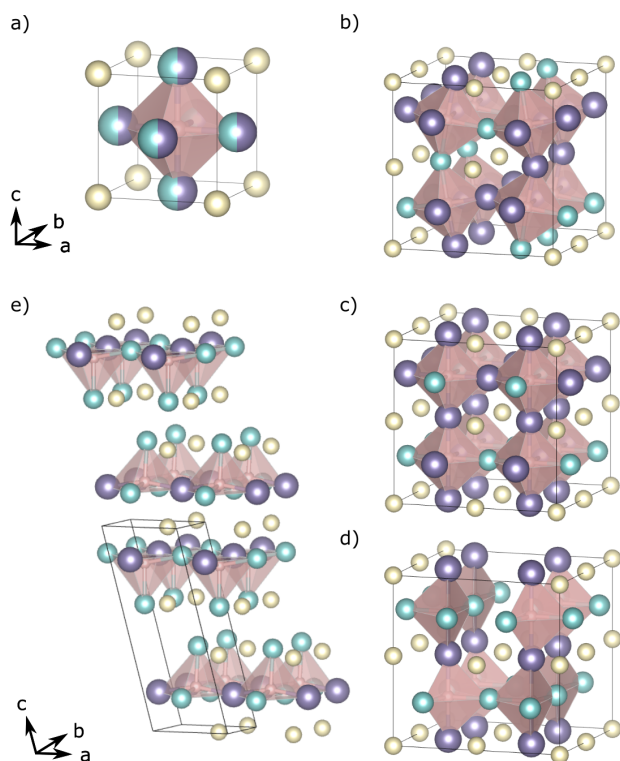


**Fig. 2** (a) The disordered cubic anti-perovskite unit cell of  $\text{Li}_2\text{FeSO}$ . (b) The  $\text{Li}_2\text{FeSO}$  structure found here. (c) The lowest energy  $\text{Li}_2\text{FeSO}$  reported previously<sup>24</sup>. (d) The structure of  $\text{Li}_2\text{Fe}_3\text{S}_2\text{O}_2$ . (e) The structure of  $\text{Li}_2\text{Fe}_4\text{S}_3\text{O}_2$ . Colour coding: cream-S, purple-Li, cyan-Fe, pink-O.

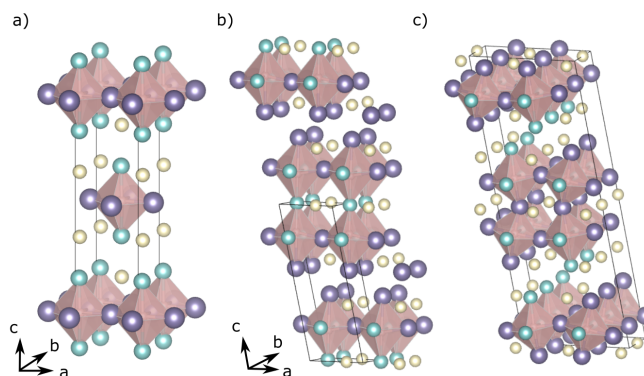


**Fig. 3** The two anti-Ruddlesden-Popper phases found in the search: (a)  $\text{Li}_2\text{Fe}_2\text{S}_2\text{O}_2$ ; (b)  $\text{Li}_4\text{Fe}_3\text{S}_3\text{O}_2$ ; (c)  $\text{Li}_4\text{Fe}_3\text{S}_3\text{O}_2$  with lower energy obtained by enumerating the Li/Fe orderings. Colour coding: cream-S, purple-Li, cyan-Fe, pink-O.

other for +2, as shown in Fig. 1. Plane wave density functional theory calculations are known to have cubic scaling, to keep the problem tractable, we limit the search to compositions with the number atoms of atoms in the empirical formula  $\leq 12$ , and the total number of atoms in the full formula  $\leq 24$ . Even with these constraints applied, there are still 33 candidate compositions to be searched. As a result, we have to perform coarse samplings of the phase space initially, where about 600 random structures generated and relaxed for each composition. Afterwards, compositions that have the lowest energy structure close to the convex are selected for further searching.

The compositions of the phases that are found to be close to the convex hull within a 50 meV per atom range is shown in Table 1, where  $V_a$  is calculated average voltage,  $\Delta V$  is the volume change after delithiation and  $E_h$  is the distance to the convex hull,  $S_c$  is the theoretical specific capacity, and  $S_e$  is the specific energy computed from on  $V_a$  and  $S_c$ . Our search has also reproduced the anti-perovskite  $\text{Li}_2\text{FeSO}$  phase (Fig. 2a) that was reported previously<sup>22</sup>, and it is predicted to be on the convex hull (e.g. thermodynamically stable) at 0 K. A previous DFT study predicts  $\text{Li}_2\text{FeSO}$  to be metastable and would decompose into  $\text{Li}_2\text{FeO}_2$ ,  $\text{FeS}$  and  $\text{Li}_2\text{S}$ <sup>24</sup>, whereas it is found to be stable here. This difference is likely to be caused by the methodology of treating transition metals in different type of compounds. In that work, the PBE/PBE+U calculations are mixed<sup>50</sup>, where the Hubbard-correction for Fe is only applied to oxide/oxysulphide phases with the energies adjusted using the correction factors from the Materials Project<sup>28</sup>. In this approach, the PBE+U correction factor is supposed to be calibrated for reproducing oxide formation energies involving metallic Fe and  $\text{O}_2$ . Applying the same term to oxysulphides would introduce systematic errors and affection the reaction energy of forming oxysulphides from oxide and sulphides. However, we found that the data and correction factors from Materials Project does not reproduce the formation energy of iron oxides using the methodologies that are referred to<sup>46,50</sup>. With refitted parameters, the PBE/PBE+U mixing approach overly favours FeS formation which could seriously affect the results. More discussion can be found in the electronic sup-

**Table 1** Compositions that are close to the convex hull found in the search and their computed average voltages and theoretical capacities. Symbols:  $V_a$  is calculated average voltage;  $\Delta V$  is the volume change after delithiation;  $E_h$  is the distance to the convex hull;  $S_c$  is the specific capacity;  $S_e$  is the specific energy.

Formula	$V_a$ (V)	$\Delta V$ (%)	$E_h$ (meV)	$S_c$ (mAh/g)	$S_e$ (Wh/kg)	Decomposition
Li <sub>2</sub> FeSO	2.3	-4.5	0.0	227.5	532.3	N/A
Li <sub>2</sub> Fe <sub>4</sub> S <sub>3</sub> O <sub>2</sub>	2.7	-7.3	0.0	146.7	398.5	N/A
Li <sub>2</sub> Fe <sub>3</sub> (SO) <sub>2</sub>	2.6	-10.0	3.4	193.1	496.0	Li <sub>2</sub> FeSO + FeO + Li <sub>2</sub> Fe <sub>4</sub> S <sub>3</sub> O <sub>2</sub>
Li <sub>2</sub> Fe <sub>2</sub> S <sub>2</sub> O	2.9	-11.7	3.4	260.6	743.6	Li <sub>2</sub> Fe <sub>4</sub> S <sub>3</sub> O <sub>2</sub> + Li <sub>2</sub> S
Li <sub>4</sub> Fe <sub>3</sub> S <sub>3</sub> O <sub>2</sub>	2.5	-3.4	18.1	248.6	633.6	Li <sub>2</sub> FeSO + Li <sub>2</sub> Fe <sub>4</sub> S <sub>3</sub> O <sub>2</sub> + Li <sub>2</sub> S
Li <sub>4</sub> Fe <sub>3</sub> S <sub>4</sub> O	2.5	-3.8	30.5	236.8	585.4	Li <sub>2</sub> Fe <sub>4</sub> S <sub>3</sub> O <sub>2</sub> + FeS + Li <sub>2</sub> S
Li <sub>2</sub> Fe <sub>4</sub> S <sub>4</sub> O	2.6	-6.9	38.6	140.5	363.4	Li <sub>2</sub> Fe <sub>4</sub> S <sub>3</sub> O <sub>2</sub> + FeS + Li <sub>2</sub> S
Li <sub>4</sub> Fe <sub>2</sub> S <sub>3</sub> O	2.1	-5.5	45.8	213.0	445.5	Li <sub>2</sub> Fe <sub>4</sub> S <sub>3</sub> O <sub>2</sub> + Li <sub>2</sub> S
Li <sub>6</sub> FeSO <sub>3</sub>	1.9	-10.0	46.3	150.9	287.3	Li <sub>2</sub> O + Li <sub>2</sub> FeO <sub>2</sub> + Li <sub>2</sub> S
Li <sub>2</sub> Fe <sub>3</sub> S <sub>3</sub> O	2.4	-7.6	48.8	182.6	446.5	Li <sub>2</sub> Fe <sub>4</sub> S <sub>3</sub> O <sub>2</sub> + FeS + Li <sub>2</sub> S
Li <sub>6</sub> FeS <sub>3</sub> O	2.3	1.6	49.9	127.8	291.5	Li <sub>2</sub> FeSO + Li <sub>2</sub> S

porting information. In this work, the Hubbard correction is applied to all Fe-containing phases including the sulphides (similar to that in the Open Quantum Material Database<sup>51</sup>). Although applying the U calibrated for oxide to sulphides may also introduce systematic errors, as the distance to hull are computed using the same set of competing phases, phases that are predicted to be close/on the convex hull should have stabilities similar to that of the Li<sub>2</sub>FeSO, which has been synthesised experimentally<sup>22</sup>.

The Li<sub>2</sub>FeSO structure found by the search here (Fig. 2b, space group *Pc*) contains Li and Fe atoms with substantial displacements from their sites in the cubic disordered anti-perovskite cell (Fig. 2a, space group *Pm* $\bar{3}$ *m*). This result can be easily rationalised by invoking our knowledge of perovskite tilting, as the O, Li, and Fe atoms have sizes such that the OLi<sub>4</sub>Fe<sub>2</sub> network contains tilted octahedra in the  $a^0b^0c^+$  pattern using the Glazer's rotation<sup>52</sup>, which is consistent the Goldschmidt tolerance factor of 0.85 computed from the ionic radii. This value is computed using weighted average of Li and Fe radii and the ionic radius of S<sup>2-</sup> in six-fold coordination. The latter may result in underestimation of the tolerance factor as S<sup>2-</sup> is in fact under an 12-fold coordination in the anti-perovskite structure. The previously reported theoretical ground state structure of Li<sub>2</sub>FeSO, which obtained by enumerating Li and Fe sites (shown in Fig. 2c, space group *P4*<sub>2</sub>*mmc*), does not have any octahedral tilting<sup>24</sup>, and it is 6 meV higher in energy compared to our structure obtained using AIRSS. This high-symmetry structure is dynamically unstable, and following the imaginary mode at the M point results in  $a^-b^-c^0$  tilted octahedra (space group *P2/c*). The final energy of this distorted structure is almost identical to the one found with AIRSS. Oxysulphides containing Fe<sup>3+</sup> are mostly unstable and far from the hull, and all of the phases in Table 1 contains Fe<sup>2+</sup> instead. This may be attributed to Fe<sub>2</sub>O<sub>3</sub> being very stable as one of the competing phases.

Several previously unknown phases have been found to be on or close to the convex hull. The Li<sub>2</sub>Fe<sub>4</sub>S<sub>3</sub>O<sub>2</sub> (space group *C2*) and Li<sub>2</sub>Fe<sub>3</sub>S<sub>2</sub>O<sub>2</sub> (space group *Pm*) are shown in Fig. 2d&e respectively. The former is on the convex hull while the latter is only 3 meV (per atom) above it. They can be regarded as cation deficient variants of anti-Ruddlesden-Popper and anti-perovskite structures. In

both cases, the oxygen atoms are pyrimidally coordinated by two Li atoms and three Fe atoms, rather than the octahedral coordination in original archetype structures. The cation deficiency can be attributed to the reduced Li-to-Fe ratio. Since a Fe<sup>2+</sup> cation carries more positive charges, fewer cations are needed to balance the negative charge of the anions. Unfortunately, the reduced Li-to-Fe ratios also means reduced specific capacities, making them less attractive as cathode materials.

On the other hand, two anti-Ruddlesden-Popper phases, Li<sub>2</sub>Fe<sub>2</sub>S<sub>2</sub>O and Li<sub>4</sub>Fe<sub>3</sub>S<sub>3</sub>O<sub>2</sub>, have been found to be close to the convex hull and more promising for cathode applications with specific capacity higher than that of the Li<sub>2</sub>FeSO. The former has a layered structure as shown in Fig. 3a, which resembles the Ruddlesden-Popper (RP) phases with a general formula A<sub>n+1</sub>B<sub>n</sub>X<sub>3n+1</sub>. The RP series can be regarded as alternating perovskite-like (ABX<sub>3</sub>) and rock salt like (AX) environments along the *z* the direction. The number *n* indicates the number of complete ABX<sub>3</sub> perovskite layers between the rock salt BX layer. In contrast to normal RP phases, such as Sr<sub>3</sub>Ru<sub>2</sub>O<sub>7</sub>, where cations take the A and B sites, here they take the anion X sites instead, and S and O occupy the A and B sites respectively. This gives the anti-Ruddlesden Popper structured oxysulphides a general formula S<sub>n+1</sub>O<sub>n</sub>(Fe/Li)<sub>3n+1</sub>. The Li<sub>2</sub>Fe<sub>2</sub>S<sub>2</sub>O phase (space group *Pc*) has *n* = 1 with one perovskite layer followed by the rock salt layer as shown in Fig. 3a, and it is only about 3 meV from the convex hull. Likewise, the Li<sub>4</sub>Fe<sub>3</sub>S<sub>3</sub>O<sub>2</sub> phase (space group *Cm*) has two perovskite layers (e.g. *n* = 2) in the unit cell, as shown in Fig. 3b. This phase is slightly less stable with a distance to hull of 18 meV per atom. Different Li/Fe orderings in the primitive cell and supercells of both phases have been enumerated, and twenty structures with the lowest electrostatic energies are further relaxed by DFT for each case. Unlike the cubic perovskite, the base structure of the RP phase is not unique, which can affect the initial rankings based on the electrostatic energies. We used the experimental structure of Sr<sub>2</sub>RuO<sub>4</sub>, Sr<sub>3</sub>Ru<sub>2</sub>O<sub>7</sub> and the structures obtained from the search as the initial templates. For Li<sub>2</sub>Fe<sub>2</sub>S<sub>2</sub>O, performing the enumeration did not generate any structure with lower energy. In fact, using the ideal Sr<sub>2</sub>RuO<sub>4</sub> structure as the template would miss the lowest energy structure that is found in the search. On the

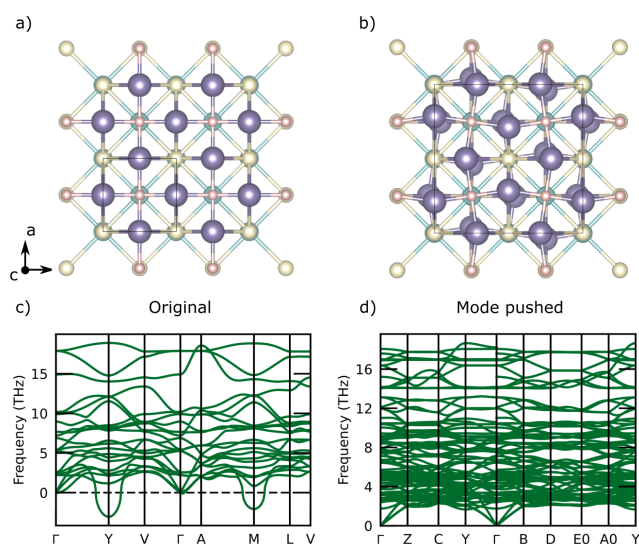


**Fig. 4** (a) The  $\text{Li}_2\text{Fe}_2\text{S}_2\text{O}$  from the search, looking down the z direction. (b) The dynamically stable  $\text{Li}_2\text{Fe}_2\text{S}_2\text{O}$  structure with rotated  $\text{OLi}_4\text{Fe}_2$  octahedra obtained by following the imaginary phonon modes. (c) The phonon band structure of  $\text{Li}_2\text{Fe}_2\text{S}_2\text{O}$  with imaginary frequencies. (d) The phonon band structure of mode-pushed  $\text{Li}_2\text{Fe}_2\text{S}_2\text{O}$ . Colour coding: cream-S, purple-Li, cyan-Fe, pink-O.

other hand, repeating the same procedure for  $\text{Li}_4\text{Fe}_3\text{S}_3\text{O}_2$  has generated many structures with lower energies by up to 14 meV per atom (distance to hull is reduced to 4 meV), and starting from the ideal structure appears to give better results. The lowest energy structure (space group  $C2/m$ ) contains  $\text{OLi}_4\text{Fe}_2$  tilted octahedra in a  $a^+b^0c^0$  tilt system, as shown in Fig. 3c.

It should be noted that many of the "above-hull" structures are in fact predicted to decompose into phases that are themselves found by the search, as shown in Table 1. If only the ternary and binary compounds in the Li-Fe-S-O chemical spaces are considered, many of them would be regarded as stable. This highlights the importance of performing a sufficient and unbiased sampling of the target chemical space for reliably predicting the thermodynamic stabilities.

To check the dynamic stability of the predicted structures, finite displacement phonon calculations have been carried out. The predicted  $\text{Li}_2\text{FeSO}$  structure was found to have no imaginary frequencies across the first Brillouin zone. The  $\text{Li}_2\text{Fe}_2\text{S}_2\text{O}$  structure obtained by the search (Fig. 3a) has a highly symmetric perovskite layer as shown in Fig. 4a. However, when we calculate the phonon band structure, it was found to have imaginary frequencies (Fig. 4c). Pushing along the imaginary mode (at  $(-0.5, 0.5, 0)$  of the conventional cell) allows us to obtain a structure with tilted  $\text{OLi}_4\text{Fe}_2$  octahedra in a  $a^0b^+c^0$  tilt system with space group  $P2_1$  (Fig. 4b). Recomputing the phonon dispersion reveals that the imaginary mode has disappeared, which can be seen in Fig. 4d. The energy per atom is reduced by about 1 meV for this distorted structure. For  $\text{Li}_4\text{Fe}_3\text{S}_3\text{O}_2$ , the lowest energy structure generated by the enumeration of symmetrically inequivalent structures (Fig. 3c) was found to be dynamically stable. Imaginary frequencies have been also found in  $\text{Li}_2\text{Fe}_3\text{S}_2\text{O}_2$

and  $\text{Li}_2\text{Fe}_4\text{S}_3\text{O}_2$ , which are subsequently eliminated by following the corresponding modes. Their final dynamically stable structures have lower energies by 2.6 meV and 0.2 meV compared with the non-distorted structures respectively, giving negligible effects for their thermodynamic stabilities. Since the structure searching was carried out with small unit cells containing symmetry operations, distortions that require increased cell sizes is not possible to be found. Nevertheless, since typically energy reduction as result of mode-pushing is small, the structures obtained directly from the search are already sufficiently accurate models for evaluating the thermodynamic stabilities. Phonon band structure for the phases mentioned above can be found in the electronic supporting information (ESI) Fig. S4.

### Electrochemical properties of the predicted phases

The average voltages, volume changes after delithiation and calculated theoretical capacities of the predicted phases are tabulated in Table 1. For Li-rich phases, only the capacity from the  $\text{Fe}^{2+}/\text{Fe}^{3+}$  redox is considered here, and Li orderings in the delithiated structures are enumerated for calculating the voltages.  $\text{Li}_2\text{FeSO}$  is found to have a voltage of 2.3 V, which is in reasonable agreement with the experimentally obtained 2.5 V. We note that for disordered materials, voltages calculated using small ordered unit cell may not be accurate, and more rigorous approaches such as cluster expansion should provide better results. The two anti-RP phases,  $\text{Li}_2\text{Fe}_2\text{S}_2\text{O}$  and  $\text{Li}_4\text{Fe}_3\text{S}_3\text{O}_2$ , are predicted to have voltages 2.9 V and 2.5 V respectively. Compared to the  $\text{Li}_2\text{FeSO}$  phase (223 mAh/g), they have higher theoretical capacities (261 mAh/g and 249 mAh/g) because their Li:Fe ratios are closer to 1:1.

The band gaps of the predicted phases are found to range between 1.8 eV to 2.2 eV using the HSE06 functional, which are a lot narrower than that of  $\text{LiFePO}_4$  (3.8 eV - 4.0 eV)<sup>53</sup>. In comparison, the band gap of  $\text{LiCoO}_2$  has been reported to range from 1.7 eV to 2.7 eV<sup>54</sup>. Hence, the new oxysulphide phases have the potential for good electronic conductivity which is desirable as cathodes. The projected density of states of the predicted phases (Fig. S5) suggest that their valence band maxima are mainly composed of Fe d states with some contributions from oxygen and sulphur p states. This confirms that the  $\text{Fe}^{2+}/\text{Fe}^{3+}$  is the main contributor to the redox capacity.

In addition to good electronic conductivity, the existence of fast lithium ion conduction pathways is also crucial for cathode materials. For  $\text{Li}_2\text{Fe}_2\text{S}_2\text{O}$ , the Li atoms only occupy the sites within the  $\text{Li}_2\text{O}$  layer of the perovskite environment as shown in Fig. 5a. Each Li is under octahedral coordination by four S atoms and two O atoms, and it has four nearest neighbour Li atoms and four next nearest neighbours. The coordination octahedron is face-sharing with the nearest neighbours and edge-sharing between the next-nearest neighbours, giving two possible kinds of migration pathways as labelled by A and B in Fig. 5a. The climbing-image nudged elastic band (NEB) method has been used to study the minimum energy pathway for a single Li vacancy to migrate. The barrier between the nearest neighbour (NN) sites is found to be 0.38 eV, and for the next-nearest neighbour (NNN) it is increased to 0.96 eV, as shown in Fig. 5c. The large difference in

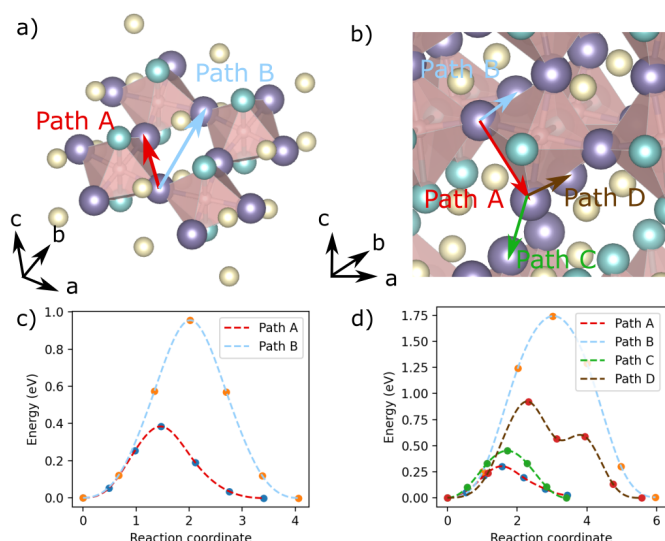


**Fig. 5** Potential Li diffusion pathways for (a)  $\text{Li}_2\text{Fe}_2\text{S}_2\text{O}$  (showing only the perovskite layer) and (b)  $\text{Li}_4\text{Fe}_3\text{S}_3\text{O}_2$  with their corresponding transition state energies (c,d) calculated using the climbing-image nudged elastic band method. Colour coding: cream-S, purple-Li, cyan-Fe, pink-O.

the barrier heights between the two cases can be understood as the former requires the Li atom to go through the face of the coordination octahedron around it, whereas the latter needs to go squeeze through the edge made of two S atoms with additional repulsion from the nearby Li atoms. In layered cathode materials, the Li atoms are known to take an indirect route through the tetragonal sites going through the faces of  $\text{LiO}_6$  octahedra, rather than the direct path through the edges<sup>55</sup>. The  $\text{Li}_4\text{Fe}_3\text{S}_3\text{O}$  structure has many inequivalent pathways, and we select representative paths connecting the nearest and next-nearest migrations in both the perovskite layer and the rock salt layer, as shown in Fig. 5b. The A and B paths correspond to the NN and NNN pathways inside the perovskite environment, and they have transition state barriers 0.30 eV and 1.74 eV respectively. The higher barrier of the NNN pathway can be attributed to the increased repulsion from the  $\text{Fe}^{2+}$  ions when compared to that in  $\text{Li}_2\text{Fe}_2\text{S}_2\text{O}$ . Path C and Path D are pathways for Li to diffuse within the rock salt layer. The former is found to have a barrier height of 0.45 eV and the latter is 0.92 eV. Unlike the diffusion in the perovskite layer, here the NN path (Path C) goes through an edge of the octahedron formed by two S atoms. We have also considered the potential pathway through the tetrahedral site coordinated by four  $\text{S}^{2-}$  in analogy to the diffusion in layered Li metal oxides. However, the Li atom is found to be not stable at that intermediate site, since after relaxations the Li atom returns to its starting position. This can be understood as the occupation of the tetrahedral site would in fact result in very short Li-Fe separation with the Fe atom in the perovskite ordered layer above/below, giving rise to increased electrostatic energies. Here, the direct oxygen-dumbbell hop of Path C is already much lower than the counterpart in  $\text{LiCoO}_2$ <sup>55</sup>, which can be attributed to larger and more polarizable  $\text{S}^{2-}$  compared with  $\text{O}^{2-}$ .

## Conclusion

The Li-Fe-O-S chemical spaces have been explored using ab initio random structure searching (AIRSS), and a series of potentially synthesisable phases that are close to or on the convex hull have been predicted. Among these candidate phases, two anti-RP structure materials  $\text{Li}_2\text{Fe}_2\text{S}_2\text{O}$  and  $\text{Li}_4\text{Fe}_3\text{S}_3\text{O}_2$  are particularly promising for cathode applications. Density functional theory calculations show that they have voltages that are similar to that of the previously reported  $\text{Li}_2\text{FeSO}$  phase, and their theoretical charge capacities exceed the latter. Fast Li conduction channels are revealed using climbing-image nudged elastic band calculations. If successfully synthesised, they can be good contenders to the commercialised  $\text{LiFePO}_4$  cathodes. Even though the low voltages ( $\sim 2.5$  V) are nowhere near that of  $\text{LiFePO}_4$ , they are compensated by much increased theoretical gravimetric capacities ( $\sim 250$  mAh/g vs  $\sim 170$  mAh/g). Our work also demonstrates that first-principles structure prediction is an effective way to explore complex quaternary chemical spaces where many new materials are waiting to be discovered for battery cathode applications and beyond.

## Conflicts of interest

There are no conflicts to declare.

## Acknowledgement

This work was supported by the Faraday Institution grant number FIRG017 and used the MICHAEL computing facilities. D. O. S. acknowledges support from the European Research Council (Grant 758345). Via our membership of the UK's HEC Materials Chemistry Consortium, which is funded by the UK Engineering and Physical Sciences Research Council (EPSRC; EP/L000202, EP/R029431, EP/T022213), this work used the ARCHER and ARCHER2 UK National Supercomputing Services. We are also grateful to the UK Materials and Molecular Modelling Hub (MMM Hub), which is partially funded by the EPSRC (EP/P020194, EP/T022213), for computational resources on the Thomas, Young and Michael supercomputers, and to UCL for access to the Myriad (Myriad@UCL) and Kathleen (Kathleen@UCL) supercomputers.

## Notes and references

- 1 K. Mizushima, P. C. Jones, P. J. Wiseman and J. B. Goodenough, *Materials Research Bulletin*, 1980, **15**, 783–789.
- 2 M. M. Thackeray, W. I. F. David, P. G. Bruce and J. B. Goodenough, *Materials Research Bulletin*, 1983, **18**, 461–472.
- 3 A. K. Padhi, K. S. Nanjundaswamy and J. B. Goodenough, *Journal of the Electrochemical Society*, 1997, **144**, 1188.
- 4 H. Huang, S.-C. Yin and L. F. Nazar, *Electrochemical and Solid-State Letters*, 2001, **4**, A170.
- 5 A. Ny n, A. Abouimrane, M. Armand, T. Gustafsson and J. O. Thomas, *Electrochemistry Communications*, 2005, **7**, 156–160.
- 6 C. Sirisopanaporn, C. Masquelier, P. G. Bruce, A. R. Armstrong and R. Dominko, *Journal of the American Chemical Society*, 2011, **133**, 1263–1265.
- 7 P. Barpanda, J.-N. Chotard, N. Recham, C. Delacourt, M. Ati, L. Dupont, M. Armand and J.-M. Tarascon, *Inorganic Chemistry*, 2010, **49**, 7401–7413.
- 8 N. Recham, J.-N. Chotard, L. Dupont, C. Delacourt, W. Walker, M. Armand and J.-M. Tarascon, *Nature Materials*, 2010, **9**, 68–74.
- 9 P. Barpanda, M. Ati, B. C. Melot, G. Rousse, J.-N. Chotard, M.-L. Doublet, M. T. Sougrati, S. A. Corr, J.-C. Jumas and J.-M. Tarascon, *Nature Materials*, 2011, **10**, 772–779.
- 10 S. Morzilli and B. Scrosati, *Electrochimica Acta*, 1985, **30**, 1271–1276.
- 11 J. Kim and A. Manthiram, *Journal of The Electrochemical Society*, 1999, **146**, 4371.
- 12 T. Matsumura, R. Kanno, Y. Inaba, Y. Kawamoto and M. Takano, *Journal of The Electrochemical Society*, 2002, **149**, A1509.

- 13 A. R. Armstrong, D. W. Tee, F. La Mantia, P. Novák and P. G. Bruce, *Journal of the American Chemical Society*, 2008, **130**, 3554–3559.
- 14 J. Kim, H. Lee, H. Cha, M. Yoon, M. Park and J. Cho, *Advanced Energy Materials*, 2018, **8**, 1702028.
- 15 J. Lee, J. K. Papp, R. J. Clément, S. Sallis, D.-H. Kwon, T. Shi, W. Yang, B. D. McCloskey and G. Ceder, *Nature Communications*, 2017, **8**, 981.
- 16 S. J. Clarke, S. G. Denis, O. J. Rutt, T. L. Hill, M. A. Hayward, G. Hyett and Z. A. Gál, *Chemistry of Materials*, 2003, **15**, 5065–5072.
- 17 N. Charles, R. J. Saballos and J. M. Rondinelli, *Chemistry of Materials*, 2018, **30**, 3528–3537.
- 18 Z. Lun, B. Ouyang, Z. Cai, R. J. Clément, D.-H. Kwon, J. Huang, J. K. Papp, M. Balasubramanian, Y. Tian, B. D. McCloskey, H. Ji, H. Kim, D. A. Kitchaev and G. Ceder, *Chem*, 2020, **6**, 153–168.
- 19 D. Deng, *ChemNanoMat*, 2017, **3**, 146–159.
- 20 R. A. House, L. Jin, U. Maitra, K. Tsuruta, J. W. Somerville, D. P. Förstermann, F. Massel, L. Duda, M. R. Roberts and P. G. Bruce, *Energy & Environmental Science*, 2018, **11**, 926–932.
- 21 S. Saha, G. Assat, M. T. Sougrati, D. Foix, H. Li, J. Vergnet, S. Turi, Y. Ha, W. Yang, J. Cabana, G. Rouse, A. M. Abakumov and J.-M. Tarascon, *Nature Energy*, 2019, **4**, 977–987.
- 22 K. T. Lai, I. Antonyshyn, Y. Prots and M. Valldor, *Journal of the American Chemical Society*, 2017, **139**, 9645–9649.
- 23 K. T. Lai, I. Antonyshyn, Y. Prots and M. Valldor, *Inorganic Chemistry*, 2018, **57**, 13296–13299.
- 24 Z. Lu and F. Ciucci, *Journal of Materials Chemistry A*, 2018, **6**, 5185–5192.
- 25 M. V. Gorbunov, S. Carrocci, S. Maletti, M. Valldor, T. Doert, S. Hampel, I. G. Gonzalez Martinez, D. Mikhailova and N. Gräßler, *Inorganic Chemistry*, 2020, **59**, 15626–15635.
- 26 J. Gamon, A. J. Perez, L. A. H. Jones, M. Zanella, L. M. Daniels, R. E. Morris, C. C. Tang, T. D. Veal, L. J. Hardwick, M. S. Dyer, J. B. Claridge and M. J. Rosseinsky, *Journal of Materials Chemistry A*, 2020, **8**, 20553–20569.
- 27 G. Ceder, *MRS Bulletin*, 2010, **35**, 693–701.
- 28 A. Jain, S. P. Ong, G. Hautier, W. Chen, W. D. Richards, S. Dacek, S. Cholia, D. Gunter, D. Skinner, G. Ceder and K. A. Persson, *APL Materials*, 2013, **1**, 011002.
- 29 G. Hautier, C. Fischer, V. Ehrlacher, A. Jain and G. Ceder, *Inorganic Chemistry*, 2011, **50**, 656–663.
- 30 T. Mueller, G. Hautier, A. Jain and G. Ceder, *Chemistry of Materials*, 2011, **23**, 3854–3862.
- 31 A. R. Oganov, C. J. Pickard, Q. Zhu and R. J. Needs, *Nature Reviews Materials*, 2019, **4**, 331.
- 32 D. J. Wales and J. P. K. Doye, *The Journal of Physical Chemistry A*, 1997, **101**, 5111–5116.
- 33 S. Goedecker, *The Journal of Chemical Physics*, 2004, **120**, 9911–9917.
- 34 A. R. Oganov and C. W. Glass, *The Journal of Chemical Physics*, 2006, **124**, 244704.
- 35 Y. Wang, J. Lv, L. Zhu and Y. Ma, *Computer Physics Communications*, 2012, **183**, 2063–2070.
- 36 C. J. Pickard and R. J. Needs, *Physical Review Letters*, 2006, **97**, 045504.
- 37 C. J. Pickard and R. J. Needs, *Journal of physics. Condensed matter : an Institute of Physics journal*, 2011, **23**, 053201–053201.
- 38 G. Henkelman, B. P. Uberuaga and H. Jónsson, *The Journal of Chemical Physics*, 2000, **113**, 9901–9904.
- 39 G. Henkelman and H. Jónsson, *The Journal of Chemical Physics*, 2000, **113**, 9978–9985.
- 40 Z. Lu, B. Zhu, B. W. B. Shires, D. O. Scanlon and C. J. Pickard, *The Journal of Chemical Physics*, 2021, **154**, 174111.
- 41 A. F. Harper, M. L. Evans and A. J. Morris, *Chemistry of Materials*, 2020, **32**, 6629–6639.
- 42 S. J. Clark, M. D. Segall, C. J. Pickard, P. J. Hasnip, M. I. J. Probert, K. Refson and M. C. Payne, *Zeitschrift für Kristallographie*, 2005, **220**, 567–570.
- 43 G. Kresse and J. Furthmüller, *Physical Review B*, 1996, **54**, 11169–11186.
- 44 G. Kresse and J. Furthmüller, *Computational Materials Science*, 1996, **6**, 15–50.
- 45 J. P. Perdew, K. Burke and M. Ernzerhof, *Physical Review Letters*, 1996, **77**, 3865–3868.
- 46 L. Wang, T. Maxisch and G. Ceder, *Physical Review B*, 2006, **73**, 195107.
- 47 A. Togo and I. Tanaka, *Scripta Materialia*, 2015, **108**, 1–5.
- 48 S. P. Huber, S. Zoupanos, M. Uhrin, L. Talirz, L. Kahle, R. Häuselmann, D. Gresch, T. Müller, A. V. Yakutovich, C. W. Andersen, F. F. Ramirez, C. S. Adorf, F. Gargiulo, S. Kumbhar, E. Passaro, C. Johnston, A. Merkys, A. Cepellotti, N. Mounet, N. Marzari, B. Kozinsky and G. Pizzi, *Scientific Data*, 2020, **7**, 300.
- 49 M. Uhrin, S. P. Huber, J. Yu, N. Marzari and G. Pizzi, *Computational Materials Science*, 2021, **187**, 110086.
- 50 A. Jain, G. Hautier, S. P. Ong, C. J. Moore, C. C. Fischer, K. A. Persson and G. Ceder, *Physical Review B*, 2011, **84**, 045115.
- 51 S. Kirklin, J. E. Saal, B. Meredig, A. Thompson, J. W. Doak, M. Aykol, S. Rühl and C. Wolverton, *npj Computational Materials*, 2015, **1**, 1–15.
- 52 A. M. Glazer, *Acta Crystallographica Section B: Structural Crystallography and Crystal Chemistry*, 1972, **28**, 3384–3392.
- 53 F. Zhou, K. Kang, T. Maxisch, G. Ceder and D. Morgan, *Solid State Communications*, 2004, **132**, 181–186.
- 54 D. Ensling, A. Thissen, S. Laubach, P. C. Schmidt and W. Jaegermann, *Physical Review B*, 2010, **82**, 195431.
- 55 A. Van der Ven and G. Ceder, *Journal of Power Sources*, 2001, **97-98**, 529–531.